

Sublattice Ferrimagnetism in Quasifreestanding Graphene

Artem G. Rybkin^{1,*}, Artem V. Tarasov¹, Anna A. Rybkina¹, Dmitry Yu. Usachov¹, Anatoly E. Petukhov¹,
Alexander V. Eryzhenkov¹, Dmitrii A. Pudikov¹, Alevtina A. Gogina¹, Ilya I. Klimovskikh^{2,1}


Giovanni Di Santo³, Luca Petaccia³, Andrei Varykhalov⁴, and Alexander M. Shikin¹

¹*St. Petersburg State University, 198504 St. Petersburg, Russia*

²*Center for Advanced Mesoscience and Nanotechnology, Moscow Institute of Physics and Technology,
141700 Dolgoprudny, Russia*

³*Elettra Sincrotrone Trieste, Strada Statale 14 km 163.5, 34149 Trieste, Italy*

⁴*Helmholtz-Zentrum Berlin für Materialien und Energie, Elektronenspeicherring BESSY II,
Albert-Einstein-Str. 15, D-12489 Berlin, Germany*

 (Received 28 December 2021; revised 17 August 2022; accepted 14 October 2022; published 22 November 2022)

We show that graphene can be magnetized by coupling to a ferromagnetic Co film through a Au monolayer. The presence of dislocation loops under graphene leads to a ferrimagnetic ordering of moments in the two C sublattices. It is shown that the band gap of ~ 80 meV in the \bar{K} point has a magnetic nature and exists for ferrimagnetic ordering. Interplay between Rashba and exchange couplings is evidenced by spin splitting asymmetry in spin-ARPES measurements and fully supported by DFT calculation of a (9×9) unit cell. Owing to sign-opposite Berry curvatures for \bar{K} and \bar{K}' valleys, the synthesized system is promising for the realization of a circular dichroism Hall effect.

DOI: [10.1103/PhysRevLett.129.226401](https://doi.org/10.1103/PhysRevLett.129.226401)

Spin splitting in graphene is required to develop graphene-based spintronic devices with low dissipation and long-distance spin transport. It can be realized by enhancement of spin-orbit and exchange interactions independently or together. Spin-orbit interaction gives rise to a number of effects such as the quantum spin Hall effect (QSHE) [1,2] and the quantum anomalous Hall effect (QAHE) [2–6], spin galvanic effect and spin Edelstein effect [7], giant Rashba effect [8,9], spin-transfer and spin-orbit torque effects [10,11], spin interference effect, etc. Existence of spin-polarized edge currents were demonstrated in a time-reversal invariant model considered by Kane and Mele [1]. It was calculated that the edge modes are in fact protected by a previously unexpected \mathbb{Z}_2 topological invariant related to Kramers degeneracy.

Magnetic proximity is a promising route to realize exchange splitting in the material [2,3,12–14], which is otherwise intrinsically non-spin-polarized. If the time-reversal symmetry is broken without external magnetic field and the system still remains topologically nontrivial, the quantum anomalous Hall effect is realized. The model of Haldane is the first example of a topological insulator beyond the quantum Hall effect [3]. It demonstrates that as long as the topological index is nonzero, one will observe all the topological phenomena expected for a quantum Hall state, including the quantized Hall conductivity and the existence of the edge states. Complex next-nearest-neighbor-hopping parameters were used in the model resulting from a nonzero periodic magnetic field with zero net flux per unit cell. Systems similar to the Haldane's

model are known as Chern insulators (average magnetic field is zero and have a strong lattice potential). Their topological characterizations are well identified by the robustness of “one-way” edge states, a nonzero Chern number and quantized conductance. It was shown that contact of graphene with antiferromagnetic (AFM) oxide gives rise to an unconventional QAHE, and the emergence of the quantum valley Hall effect (QVHE) for magnetization lying in the plane [6]. In case of zero Chern numbers and opposite Berry curvatures for \bar{K} and \bar{K}' valleys, a circular dichroism Hall effect and the Dirac Mott insulator state were theoretically predicted recently in an antiferromagnetic superatomic graphene [15].

In our previous work [16], it was reported a realization of magneto-spin-orbit graphene on Au/Co interface with dislocation loops, but due to the large unit cell of this reconstruction, constrained density functional theory calculation (DFT) of a (2×2) unit cell was performed. It was shown that exchange coupling in graphene with giant Rashba splitting leads to spin splitting asymmetry at opposite \bar{K} and \bar{K}' points. Our finding of giant Rashba splitting in graphene on Au/Co interface that agrees with previous experiments [8,9,13] is in contrast with DFT calculations in Refs. [17–19] but our results were clearly supported by DFT calculations of Gr/Ni system with intercalated Au clusters [20] and tight-binding calculations of graphene on top of a gold monolayer in the hcp configuration [21]. It was concluded in Refs. [17–19] that sizable spin splittings become giant (~ 60 – 100 meV) only near avoided-crossing gaps. Reference [19] claims that

experimental spin splitting magnitudes are determined by the magnetic coupling with the metal surface and not by the spin-orbit coupling.

In the current Letter, we address the long-standing problem of giant spin-orbit and exchange splittings in graphene associated with the necessity of DFT calculations of large-scale structures (including misfit dislocations) for a correct description of graphene magnetization and an explanation of the experimental data. We investigate magneto-spin-orbit graphene by DFT and by spin- and angle-resolved photoelectron spectroscopy (spin-ARPES) to understand the mechanism of exchange field transfer to graphene at enlarged distance. We also clearly define the role that the dislocation loops are expected to play in the field transfer and in sublattice ferrimagnetism in a honeycomb lattice.

ARPES and spin-ARPES measurements were performed at the Resource Center “Physical Methods of Surface Investigation” (RC PMSI) of SPbU Research park, the BaDEIPh beam line [22] of the Elettra synchrotron, and the UE112_PGM-1 beam line of BESSY II synchrotron (HZB Berlin) on samples kept at room temperature. A narrow-band UV He-discharge light source VG Scienta VUV 5k was used in the Nanolab setup at the RC PMSI. Epitaxial well-oriented graphene grown on the Co(0001)/W(110) by chemical vapor deposition was intercalated with the Au monolayer. The synthesized sample was magnetized in plane along the easy magnetization axis of Co thin film (i.e., perpendicular to the direction of the ARPES measurements which was along $\bar{\Gamma}\bar{K}$). More details on sample preparation, ARPES, spin-ARPES and theoretical calculations are explained in Sec. A of Ref. [23].

First of all, we report the experimental characterization of fully intercalated graphene by low energy electron diffraction (LEED), ARPES and spin-ARPES measurements. Figure 1(b) shows the LEED pattern with a superstructure periodicity of $\sim(9 \times 9)$ and diffraction spots up to the second order. It is well known that the Au monolayer is alloyed with Ni or Co with formation of dislocation loops with $(9-10) \times (9-10)$ lateral periodicity [16,43,44]. In Figs. 1(a) and 1(c), we plot the ARPES intensity maps in the $\bar{\Gamma}\bar{K}$ direction of the surface Brillouin zone. The following characteristic features were found: band gap opening (E_g) of 80 ± 25 meV [Figs. 1(c) and 1(d)] and asymmetric spin splitting of the π band near the \bar{K} point for opposite magnetization directions. The spin splitting is shown by blue and red arrows in Fig. 1(e) and amounts to 40 ± 10 and 80 ± 10 meV for “upwards” and “downwards” cobalt magnetization directions, respectively. The magnetization is perpendicular to the $\bar{\Gamma}\bar{K}$ direction (parallel to the k_y axis) and the cobalt layer has no other magnetic domains (see Sec. B of Ref. [23]). A change in the direction of magnetization by rotating the sample by 180° around the surface normal is equivalent to remagnetizing the sample and therefore to measuring at the opposite \bar{K} and \bar{K}' points

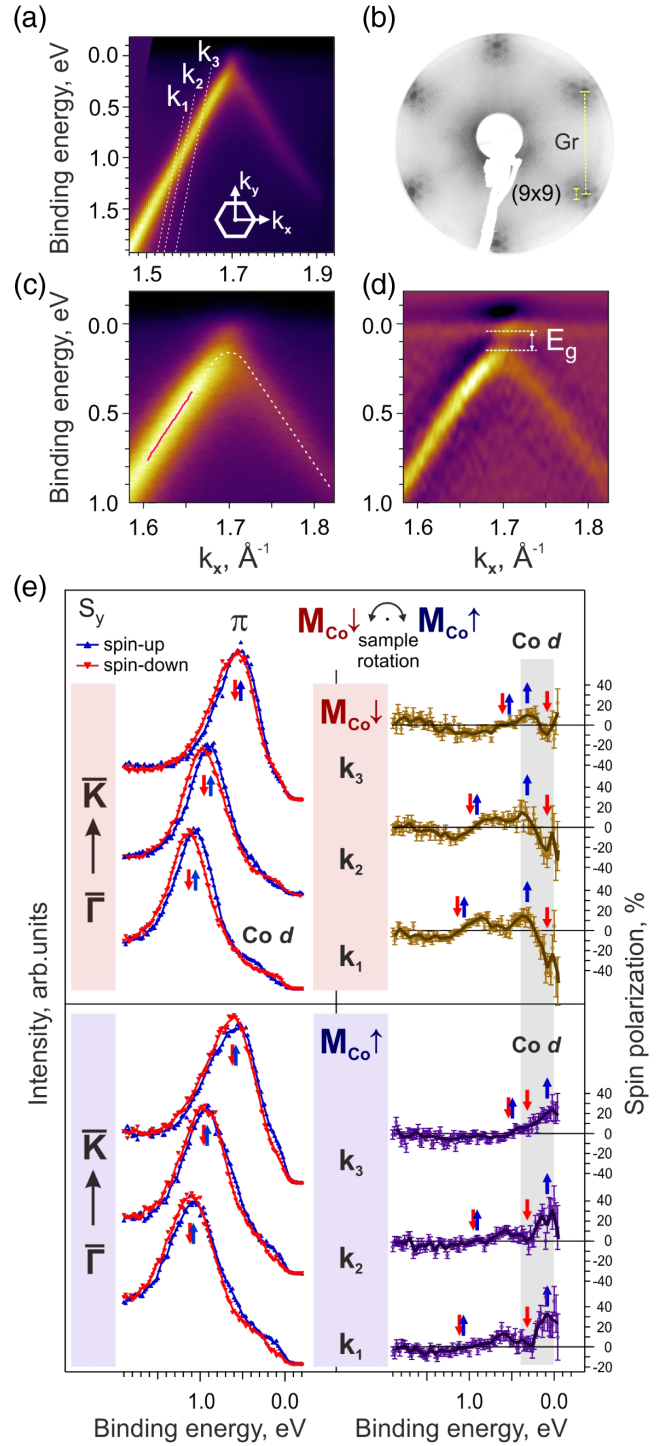


FIG. 1. (a) ARPES intensity map for the π band, including the enlarged map (c) and its second derivative with respect to energy (d). Solid red line shows the result of momentum distribution curves fitting with Lorentzian peak function. (b) LEED pattern of the epitaxial $\sim(9 \times 9)$ graphene superlattice formed on the Au/Co(0001) interface. (e) Spin-ARPES spectra (with the spin polarizations on the right side) of Gr/Au/Co(0001)/W(110) system measured at k_1 , k_2 , and k_3 momenta in (a) and for opposite magnetization directions obtained by 180° sample rotation. The photon energy is 21.2 eV.

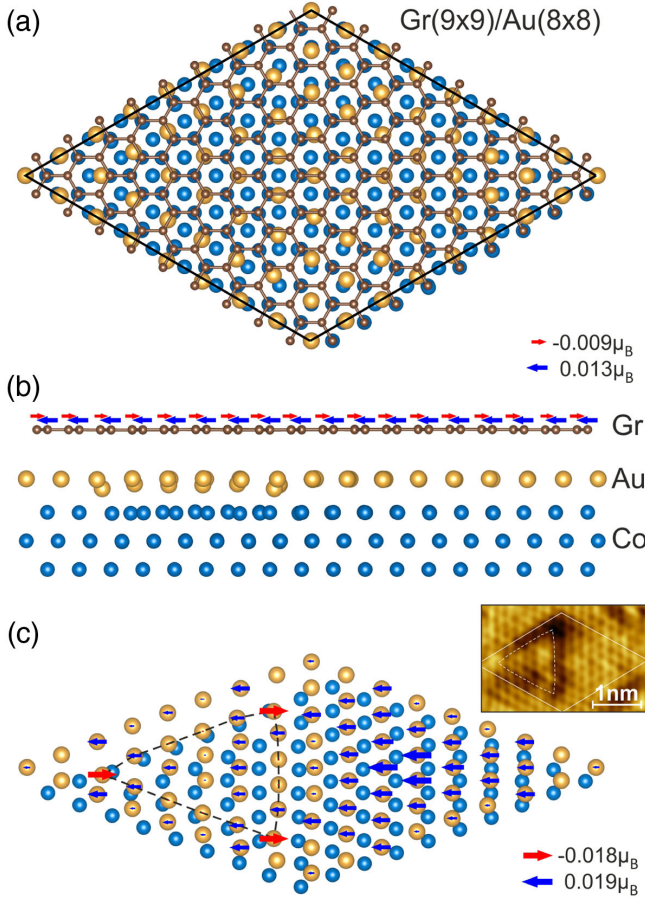


FIG. 2. Relaxed unit cell of Gr/Au/Co structure with dislocation loop: top view (a), side view (b), and isometric view of Au-Co dislocation loop under graphene (c). The dislocation loop is marked by a dotted line in panel (c) and on the inserted STM image. Sizes of the arrows are proportional to atomic magnetic moment values on gold and carbon atoms. The arrows indicating the maximum magnetic moments in two opposite directions for graphene and Au-Co dislocation loop are included in the legends. The direction of Co layer magnetization points to the right. The unit cell drawings are produced by VESTA software [48].

(Sec. B of Ref. [23]). In this case, the magnetization of the cobalt layer remains constant, only its in-plane component is reversed in sign. The asymmetric picture of the spin splitting with the same sign of spin polarization [Fig. 1(e)] suggests that the spin-orbit splitting predominates over the exchange one [45]. Otherwise, the polarization curve would change sign for π states, as for Co d states, with a change in magnetization.

In order to explain the obtained spin splitting asymmetry, DFT calculations for a large unit cell Gr(9×9)/Au(8×8) were performed. Figure 2 shows the result of structural relaxation of the unit cell with five absent atoms in the Co layer nearest to the Au layer (see details in Sec. C of Ref. [23]), which is consistent with the scanning tunneling microscopy (STM) data shown in the inset in Fig. 2(c). It clearly reveals the formation of misfit dislocation at the

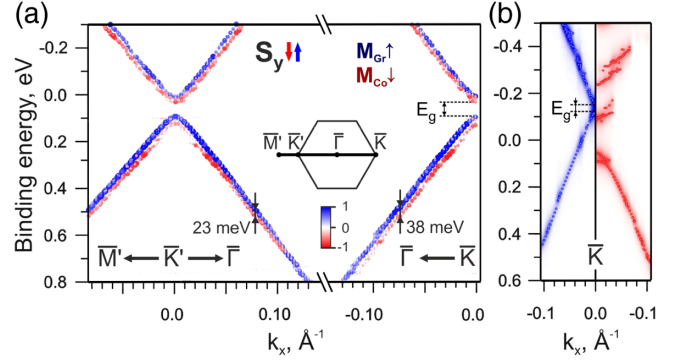


FIG. 3. (a) The unfolded (9×9) band structure of Gr/Au/Co around the opposite \bar{K}' and \bar{K} points. The symbol size and color represent the Bloch spectral weight for S_y spin component. (b) The unfolded (9×9) graphene band structure of Gr/Au/Co without dislocation loop. Spectral weights were used for the ARPES simulation in which the bands were broadened using a Lorentzian function with a half width of 0.02 eV. Cobalt layer was magnetized in-plane perpendicular to the $\bar{\Gamma}\bar{K}(\bar{K}')$ direction in both calculations. $M_{\text{Gr}\uparrow}$ and $M_{\text{Co}\downarrow}$ denote the magnetization directions of graphene and cobalt layers, respectively.

Au-Co interface with Au atoms displaced toward the Co layer at the corners of the triangular loop as in the case of Au on Ni(111) [43,44]. Band structure calculations for this relaxed unit cell shown in Fig. 3(a) reveal the formation of the band gap E_g of about 60 meV at the Dirac point. Comparing the spin splitting near \bar{K} and \bar{K}' , a splitting asymmetry (23 vs. 38 meV at 0.5 eV of binding energy) can be seen. However, it is smaller than that obtained in the experiment, indicating a smaller spin-orbit contribution to the spin splitting in the calculation. The value of spin-orbit splitting of ~ 7.5 meV estimated from the calculation is consistent with the previously reported values at the equilibrium distance between Gr and Au of ~ 3.3 – 3.5 Å [8,17,19]. In Fig. 1(e), one can note that spin polarization for the π state is not reversed with magnetization in the experiment. For this case, spin-orbit splitting is about 60 ± 10 meV and exchange splitting is about 20 ± 10 meV. We suppose that a phonon-assisted spin-orbit splitting due to electron-phonon interactions [46,47] may be responsible for the underestimated spin-orbit splitting in the calculation results.

It was surprising that ferrimagnetic (FIM) ordering was observed in Gr and Au layers (calculated atomic magnetic moments are shown by blue and red arrows in Fig. 2). Despite the difference in magnitude of magnetic moments on the gold atoms, the atomic magnetic moments on graphene sublattices have a uniform distribution with an accuracy of $0.001 \mu_B$.

To provide further evidence for the FIM nature of the band gap and the relation between FIM ordering and dislocation loop structure, we carried out DFT calculations of the (9×9) unit cell, but without dislocation loop

[Fig. 3(b)]. The unit cell was constructed on the basis of the initial one with Gr-Au distance set to 3.36 Å. In this case, the Dirac point band gap (see spin-down states of graphene) is about half of that for the structure with dislocation loops due to suppression of sublattice ferrimagnetism (magnetic moments on graphene atoms of *A* and *B* sublattices have the same sign and are close to 0.002 and 0.007 μ_B). At the same time, strong hybridization is observed for spin-up states of graphene and cobalt in the region of the Dirac point. A similar hybridization between graphene and cobalt states was observed earlier for the (2×2) unit cell of Gr/Au/Co [16]. Calculation of the band structure of graphene with the distance between graphene and gold monolayer reduced by 0.2 Å from the equilibrium distance (Sec. D of Ref. [23]) also confirms the magnetic nature of the band gap. In this case, the values of the magnetic moments on graphene atoms are decreased by two orders of magnitude and the band gap turns out to be closed.

To better understand the band structure of FIM graphene, we reproduce AFM, FIM, and ferromagnetic (FM) states by a tight-binding model in graphene (see Sec. E of Ref. [23]) and compare the FIM band structures with DFT results. The effective Hamiltonian can be written as

$$H = -t \sum_{\langle i,j \rangle \alpha} (\hat{c}_{i\alpha}^\dagger \hat{c}_{j\alpha} + \text{H.c.}) + U \sum_i (\hat{n}_{i\uparrow} n_{i\downarrow} + \hat{n}_{i\downarrow} n_{i\uparrow}) + it_R \sum_{\langle i,j \rangle \alpha, \alpha'} (\hat{c}_{i\alpha}^\dagger [\boldsymbol{\sigma}_{\alpha\alpha'}^s \times \tilde{\mathbf{d}}_{ij}]_z \hat{c}_{j\alpha'} - \text{H.c.}),$$

where i, j labels nearest neighbor sites in sublattice *A* (*B*), the fermionic operator $\hat{c}_{i\alpha}^\dagger$ ($\hat{c}_{i\alpha}$) creates (annihilates) an electron at i site of spin α (\uparrow, \downarrow), and similar for site j , t is the hopping parameter, U is the strength of on-site electron repulsion, which mimics the exchange interaction with the substrate, $\hat{n}_{i\alpha}$ is the spin density operator ($\hat{n}_{i\alpha} = \hat{c}_{i\alpha}^\dagger \hat{c}_{i\alpha}$) and $n_{i\alpha}$ is the mean-field occupation number, t_R is the Rashba spin-orbit coupling constant with \mathbf{d}_{ij} being a lattice vector pointing from site j to site i ($\tilde{\mathbf{d}}_{ij}$ is a corresponding unit vector), and $\boldsymbol{\sigma}^s$ is a vector of Pauli matrices.

Three cases of graphene magnetization are possible with model Hamiltonian as shown in Fig. 4: AFM, FIM, and FM. Obviously, AFM ordering leads to the opening of the band gap. On the other hand, the presence of nonzero magnetization of graphene in the FIM phase leads to a decrease of the gap value, which is completely closed in the FM phase, but exchange splitting is enhanced with the magnetization. The main difference between AFM and FIM phases with Rashba interaction is related to the absence or presence of spin splitting asymmetry near the \bar{K} (\bar{K}') points. Figure 4(d) shows the tight-binding calculation results with weak and strong Rashba interaction that are in the best agreement with the DFT and experimental results (see details in Sec. E of Ref. [23]). One has competing contributions of Rashba and exchange

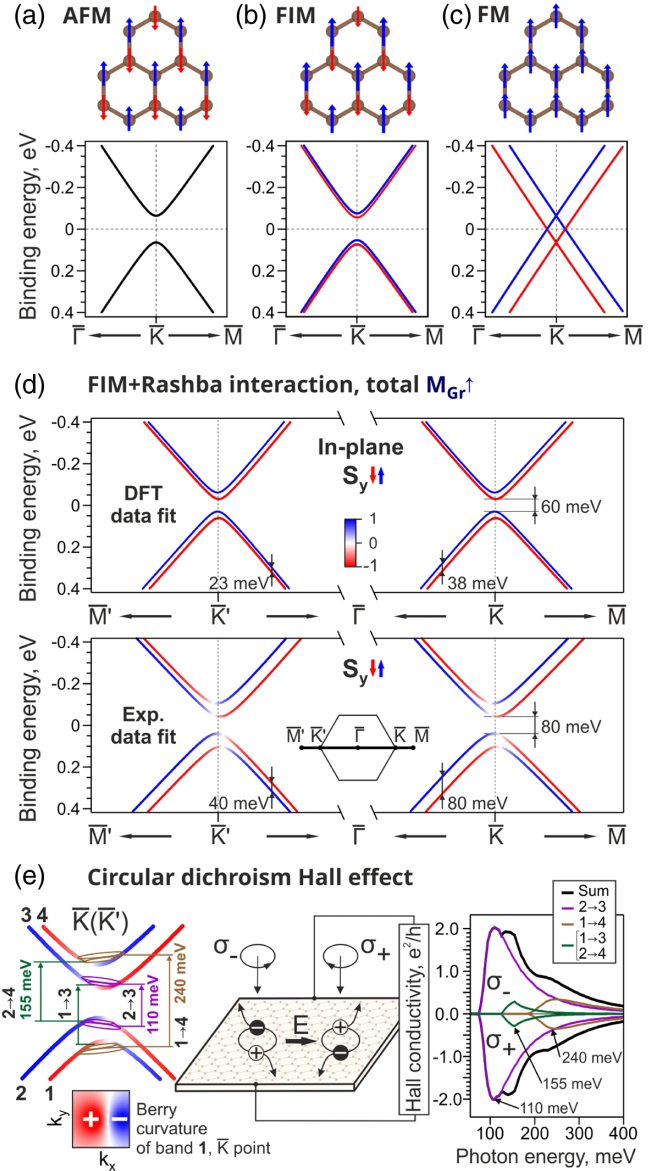


FIG. 4. The band structures calculated around the \bar{K} (\bar{K}') points using a model Hamiltonian for different graphene magnetizations and without spin-orbit interaction: AFM (a), FIM (b), and FM (c). Panel (d) shows the FIM case with Rashba interaction to fit the DFT and experimental data. (e) Schematic illustration of circular dichroism Hall effect with left-handed (σ_-) and right-handed (σ_+) light polarizations. The maxima on the Hall conductivity curve are observed due to the inclusion of new interband transitions with increasing the photon energy. A square line shape with $\Delta E/\hbar\omega = 10\%$ was set for the model curve of power spectral density.

interactions that result in the spin splitting asymmetry relative to the $\bar{\Gamma}$ point.

Using the tight-binding Hamiltonian with fitted parameters, Berry curvatures and Chern numbers were calculated for in-plane magnetization to analyze the implementation of Hall effects (Sec. E of Ref. [23]). In spite of the Chern numbers being zero, the Berry curvatures for all bands

share the dipolar structure and has opposite signs for \bar{K} and \bar{K}' valleys. The calculation of the Hall conductivity [Fig. 4(e)] taking into account the probability of optical transitions showed the presence of a robust Hall effect using circular polarized light. This phenomenon is associated with the presence of a dipole structure of Berry curvatures near the $\bar{K}(\bar{K}')$ points and nonequal spin-up and spin-down photoexcitation rates in these regions.

In summary, we showed the existence of FIM ordering in n-type doped graphene on Au/Co interface with dislocation loops that are responsible for the uniform magnetizations on graphene sublattices. The band gap at the Dirac point was revealed by ARPES and DFT methods. Tight-binding calculation results are in good agreement with the spin-ARPES data, showing the possibility of implementation of the circular dichroism Hall effect.

A. G. R., A. A. R., D. Yu. U., A. A. G., I. I. K., and A. M. S. acknowledge St. Petersburg State University (SPbU) for Research Grant No. 90383050. This work was supported by Russian Science Foundation Grants (No. 20-72-00031 in the part of *ab initio* calculations and No. 18-12-00062 in the part of synthesis and ARPES measurements with the use of synchrotron radiation), RFBR project No. 20-32-70127 (in the part of ARPES and spin-ARPES measurements with the use of laboratory sources, analysis of experimental data) and the Russian German Laboratory at BESSY II. A. V. T. acknowledge the support by the German-Russian Interdisciplinary Science Center (G-RISC) funded by the German Federal Foreign Office via the German Academic Exchange Service (DAAD). We thank Elettra Sincrotrone Trieste for providing access to its synchrotron radiation facilities.

* artem.rybkin@spbu.ru

- [1] C. L. Kane and E. J. Mele, *Phys. Rev. Lett.* **95**, 146802 (2005).
- [2] V. T. Phong, N. R. Walet, and F. Guinea, *2D Mater.* **5**, 014004 (2017).
- [3] F. D. M. Haldane, *Phys. Rev. Lett.* **61**, 2015 (1988).
- [4] Z. Qiao, S. A. Yang, W. Feng, W.-K. Tse, J. Ding, Y. Yao, J. Wang, and Q. Niu, *Phys. Rev. B* **82**, 161414(R) (2010).
- [5] M. Offidani and A. Ferreira, *Phys. Rev. Lett.* **121**, 126802 (2018).
- [6] H. Takenaka, S. Sandhoefner, A. A. Kovalev, and E. Y. Tsymbal, *Phys. Rev. B* **100**, 125156 (2019).
- [7] L. Li, J. Zhang, G. Myeong, W. Shin, H. Lim, B. Kim, S. Kim, T. Jin, S. Cavill, B. S. Kim, C. Kim, J. Lischner, A. Ferreira, and S. Cho, *ACS Nano* **14**, 5251 (2020).
- [8] D. Marchenko, A. Varykhalov, M. R. Scholz, G. Bihlmayer, E. I. Rashba, A. Rybkin, A. M. Shikin, and O. Rader, *Nat. Commun.* **3**, 1232 (2012).
- [9] A. M. Shikin, A. G. Rybkin, D. Marchenko, A. A. Rybkina, M. R. Scholz, O. Rader, and A. Varykhalov, *New J. Phys.* **15**, 013016 (2013).
- [10] A. M. Shikin, A. A. Rybkina, A. G. Rybkin, I. I. Klimovskikh, P. N. Skirdkov, K. A. Zvezdin, and A. K. Zvezdin, *Appl. Phys. Lett.* **105**, 042407 (2014).
- [11] A. A. Rybkina, A. G. Rybkin, I. I. Klimovskikh, P. N. Skirdkov, K. A. Zvezdin, A. K. Zvezdin, and A. M. Shikin, *Nanotechnology* **31**, 165201 (2020).
- [12] A. G. Swartz, P. M. Odenthal, Y. Hao, R. S. Ruoff, and R. K. Kawakami, *ACS Nano* **6**, 10063 (2012).
- [13] A. Varykhalov, J. Sánchez-Barriga, D. Marchenko, P. Hlawenka, P. S. Mandal, and O. Rader, *Nat. Commun.* **6**, 7610 (2015).
- [14] D. V. Averyanov, I. S. Sokolov, A. M. Tokmachev, O. E. Parfenov, I. A. Karateev, A. N. Taldenkov, and V. G. Storchak, *ACS Appl. Mater. Interfaces* **10**, 20767 (2018).
- [15] Y. Zhou and F. Liu, *Nano Lett.* **21**, 230 (2021).
- [16] A. G. Rybkin, A. A. Rybkina, M. M. Otrokov, O. Y. Vilkov, I. I. Klimovskikh, A. E. Petukhov, M. V. Filianina, V. Y. Voroshnin, I. P. Rusinov, A. Ernst, A. Arnau, E. V. Chulkov, and A. M. Shikin, *Nano Lett.* **18**, 1564 (2018).
- [17] J. Sławińska and J. I. Cerdá, *Phys. Rev. B* **98**, 075436 (2018).
- [18] E. Voloshina and Y. Dedkov, *Adv. Theory Simul.* **1**, 1800063 (2018).
- [19] J. Sławińska and J. I. Cerdá, *New J. Phys.* **21**, 073018 (2019).
- [20] M. Krivenkov, E. Golias, D. Marchenko, J. Sánchez-Barriga, G. Bihlmayer, O. Rader, and A. Varykhalov, *2D Mater.* **4**, 035010 (2017).
- [21] A. López, L. Colmenárez, M. Peralta, F. Mireles, and E. Medina, *Phys. Rev. B* **99**, 085411 (2019).
- [22] L. Petaccia, P. Vilmercati, S. Gorovikov, M. Barnaba, A. Bianco, D. Cocco, C. Masciovecchio, and A. Goldoni, *Nucl. Instrum. Methods Phys. Res., Sect. A* **606**, 780 (2009).
- [23] See Supplemental Material at <http://link.aps.org/supplemental/10.1103/PhysRevLett.129.226401> for details of sample preparation, ARPES, spin-ARPES, and theoretical calculations, which includes Refs. [24–42].
- [24] D. Usachov, A. Fedorov, M. M. Otrokov, A. Chikina, O. Vilkov, A. Petukhov, A. G. Rybkin, Y. M. Koroteev, E. V. Chulkov, V. K. Adamchuk, A. Grneis, C. Laubschat, and D. V. Vyalikh, *Nano Lett.* **15**, 2396 (2015).
- [25] D. Y. Usachov, K. A. Bokai, D. E. Marchenko, A. V. Fedorov, V. O. Shevelev, O. Y. Vilkov, E. Y. Kataev, L. V. Yashina, E. Rhl, C. Laubschat, and D. V. Vyalikh, *Nanoscale* **10**, 12123 (2018).
- [26] M. H. Kang, S. C. Jung, and J. W. Park, *Phys. Rev. B* **82**, 085409 (2010).
- [27] G. K. H. Madsen, P. Blaha, K. Schwarz, E. Sjöstedt, and L. Nordström, *Phys. Rev. B* **64**, 195134 (2001).
- [28] P. Blaha, K. Schwarz, F. Tran, R. Laskowski, G. K. H. Madsen, and L. D. Marks, *J. Chem. Phys.* **152**, 074101 (2020).
- [29] J. P. Perdew, K. Burke, and M. Ernzerhof, *Phys. Rev. Lett.* **77**, 3865 (1996).
- [30] O. Rubel, A. Bokhanchuk, S. J. Ahmed, and E. Assmann, *Phys. Rev. B* **90**, 115202 (2014).
- [31] J. Hubbard and B. H. Flowers, *Proc. R. Soc. A* **276**, 238 (1963).
- [32] Y. Claveau, B. Arnaud, and S. Matteo, *Eur. J. Phys.* **35**, 035023 (2014).

- [33] T. O. Wehling, E. Şaşoğlu, C. Friedrich, A. I. Lichtenstein, M. I. Katsnelson, and S. Blügel, *Phys. Rev. Lett.* **106**, 236805 (2011).
- [34] R. Resta, *J. Phys. Condens. Matter* **12**, R107 (2000).
- [35] J. Sinova, T. Jungwirth, J. Kučera, and A. H. MacDonald, *Phys. Rev. B* **67**, 235203 (2003).
- [36] L. C. Lew Yan Voon and L. R. Ram-Mohan, *Phys. Rev. B* **47**, 15500 (1993).
- [37] G. Sundaram and Q. Niu, *Phys. Rev. B* **59**, 14915 (1999).
- [38] S. Chaudhary, C. Knapp, and G. Refael, *Phys. Rev. B* **103**, 165119 (2021).
- [39] E. A. A. Pogna *et al.*, *ACS Nano* **15**, 11285 (2021).
- [40] F. Rana, P. A. George, J. H. Strait, J. Dawlaty, S. Shivaraman, M. Chandrashekar, and M. G. Spencer, *Phys. Rev. B* **79**, 115447 (2009).
- [41] T. Ozaki, *Phys. Rev. B* **67**, 155108 (2003).
- [42] P. Kurz, F. Förster, L. Nordström, G. Bihlmayer, and S. Blügel, *Phys. Rev. B* **69**, 024415 (2004).
- [43] L. P. Nielsen, The nucleation and growth of Au on Ni(110) and Ni(111): A scanning tunneling microscopy study, Ph.D. thesis, University of Aarhus, 1995.
- [44] J. Jacobsen, L. P. Nielsen, F. Besenbacher, I. Stensgaard, E. Lægsgaard, T. Rasmussen, K. W. Jacobsen, and J. K. Nørskov, *Phys. Rev. Lett.* **75**, 489 (1995).
- [45] D. Yu. Usachov, M. Güttler, S. Schulz, G. Poelchen, S. Seiro, K. Kliemt, K. Kummer, C. Krellner, C. Laubschat, E. V. Chulkov, and D. V. Vyalikh, *Phys. Rev. B* **101**, 245140 (2020).
- [46] B. Monserrat and D. Vanderbilt, arXiv:1711.06274v1.
- [47] M. Schlipf and F. Giustino, *Phys. Rev. Lett.* **127**, 237601 (2021).
- [48] K. Momma and F. Izumi, *J. Appl. Crystallogr.* **44**, 1272 (2011).